

A Time-Synchronized Video Reference System for Data Analysis of Body-Attached Sensor Nodes in Outdoor Scenarios

Lukas Schulthess ¹, Fabian Pleisch ¹, Matheo Käch ³

Björn P. Bruhin ^{2,3}, Michele Magno ¹, Luca Benini ¹, Christoph Leitner ¹

¹ Department of Information Technology and Electrical Engineering, ETH Zurich, Zurich, Switzerland

² Swiss Federal Institute of Sport Magglingen, Magglingen, Switzerland

³ Swiss-Ski, Worblaufen, Switzerland

Abstract—Wearable body-attached multi-sensor systems enable detailed analysis of human motion and physiological signals in sports, rehabilitation, and movement research. While wireless synchronization techniques can reliably align sensor data streams, interpreting and validating complex or unconstrained activities often requires an additional, objective visual reference. Existing laboratory-grade reference systems provide high accuracy but are impractical for outdoor or field deployments. In contrast, commercial video timecode solutions typically rely on local device-to-device synchronization, which increases the power required to maintain synchronization. This is not desirable in many application scenarios. This paper presents a lightweight Timecode Generator (TCG) that converts Global Navigation Satellite System (GNSS)-derived time directly into a Linear Timecode (LTC) signal that is injected into the recording via a camera audio channel. The approach eliminates continuous handshaking, allowing the system to be activated immediately before the action of interest, thus reducing power consumption and enabling smaller batteries and unobtrusive hardware designs of body-attached sensor nodes. The TCG supports common video frame rates of 24, 25, and 30 frames per second (fps). Experimental evaluation confirms that accurate time alignment is maintained for several minutes without GNSS updates. At 30 fps, the alignment duration is 543 s before a potential frame-level shift occurs. With an average power consumption of 35.37 mW, the system achieves an operating time of up to 75 h when powered by two standard AAA alkaline batteries.

Index Terms—GNSS Time Synchronization, Clock Synchronization, Time Drift, Linear Time Code, Camera Synchronization, Wearable Sensing, Hyperconnected Body

I. INTRODUCTION

Wearable, body-attached multi-sensor systems have become a key technology for capturing human motion and physiological signals. By combining data from multiple wearable sensing devices positioned at different body locations, such as wrist [1], knee [2], or torso [3], in-depth situational or motion analysis is enabled. This spatial distribution of sensing locations increases information density and improves situational awareness compared to single-device or single-location approaches. Such systems are widely used in sports performance analysis [4], rehabilitation [5], and general movement analysis [6] for post-action data investigation and interpretation.

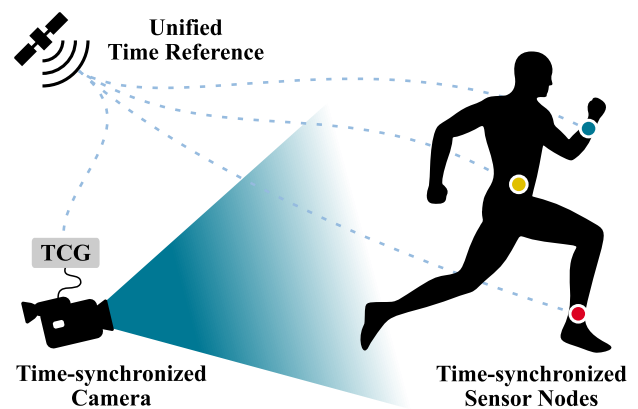


Fig. 1. Multiple body-worn devices, time-synchronized via GNSS, record data during outdoor activities. To provide a visual ground truth and a temporal reference for post-event analysis using consumer-grade cameras, a dedicated Timecode Generator (TCG) has been developed to embed precise timing information into each recorded video frame.

However, while data collected from multiple body locations can already provide valuable insights, the full potential of multi-sensor systems is realized only when all sensor data streams are precisely aligned on a common time axis. Accurate temporal synchronization enables joint analysis of multi-location sensor data to provide a holistic view of complex motion patterns. To achieve this, wearable sensor nodes are commonly synchronized between each other using wireless short-range protocols such as Bluetooth low energy (BLE) [7]–[9] or Enhanced ShockBurst [10], achieving synchronization accuracy below 1 ms by regularly exchanging synchronization packets. This ensures that dynamic events are accurately aligned across all sensor data streams and enable precise temporal correlation and on-device processing or post-action analyses [11].

Despite synchronized sensing, data analysis remains challenging when relevant features are not clearly identifiable from the sensor data alone [12]. This is often the case in unconstrained environments, when activities are unknown or when motion sequences are complex. Interpreting sensor data in a movement context requires a camera-based visual ground-truth reference, which in turn necessitates accurate temporal

synchronization between the camera stream and sensor nodes. This can be achieved by embedding time information directly into the video stream. Using LTC [13], timing data can be injected via the camera’s audio channel. Several commercial systems adopt this approach, with synchronization established through dedicated handshake procedures between devices [14]–[16]. In these setups, the unified time reference is typically obtained from a master device, often a smartphone, and distributed to all devices. Synchronization must then be maintained after the initial handshake throughout the recording period, which increases the system’s power consumption.

In contrast, body-worn sensor systems must be compact, lightweight, and unobtrusive to avoid interfering with the wearer’s natural movement, imposing strict limits on battery capacity. In outdoor scenarios such as ski jumping, there can be a substantial delay between the initial synchronization handshake of the camera and sensor node and the onset of the activity of interest [17]. Maintaining synchronization during this idle period drains battery resources, thereby reducing the system’s operational lifetime [18]. Another way to achieve synchronization is to use a GNSS-based time reference instead of a device-to-device handshake. This approach eliminates the need for direct coordination between devices, as cameras and body-attached sensor nodes independently align their data streams using a common satellite-provided time source, as shown in Fig. 1. As a result, the camera and sensor nodes can be powered on immediately before the action of interest for synchronization with the GNSS time base, thus reducing the active time of all system components and overall power consumption. This allows the use of smaller batteries and lighter hardware while improving usability in field deployments.

In this context, we present a portable, lightweight TCG that generates LTC-encoded timestamps directly from GNSS-derived satellite time, without requiring any external synchronization equipment. Combined with GNSS-synchronized body-attached sensor nodes, this system enables synchronized video and sensor data collection by relying on a common GNSS-based time source. In particular, this article presents the following contributions:

- 1) **Timecode Generator:** A compact, standalone system that generates LTC signals derived from GNSS-based time information, specifically tailored for the microphone inputs of consumer-grade video cameras.
- 2) **Multi-frame-rate support:** User-selectable frame rates of 24, 25, and 30 fps, with adjustable output amplitude in the range of 1 mV to 50 mV to accommodate the microphone input requirements of consumer-grade cameras.
- 3) **Timing Analysis:** A detailed timing analysis verifies the precise and correct generation of LTC signals and quantifies the duration for which synchronization remains stable in the absence of GNSS updates.

II. BACKGROUND & RELATED WORK

Linear Timecode (LTC) is a standardized and widely adopted method for time-stamping video recordings in professional audio-visual production and broadcast systems [13].

It encodes absolute time information as an audio signal that is recorded alongside the video on a conventional audio channel, typically injected via the microphone input. By embedding timing information directly into the audio stream, LTC enables time recovery of hour, minute, second, and frame number information for each video frame during post-processing.

During post-processing, the encoded timestamps can be extracted from the audio stream using dedicated software, such as the open-source library *libLTC* [19]. Owing to its simplicity, robustness, and compatibility with consumer and mid-range commercial recording equipment, LTC is well suited for time-synchronized multimedia acquisition and distributed measurement systems. Each LTC frame consists of a fixed-length 80-bit word. Of these, 26 bits encode the timestamp in the format *frame:second:minute:hour*. An additional 32 bits are reserved for user-defined data fields, referred to as binary groups, which may contain auxiliary metadata such as recording date or geographic information. The remaining bits are allocated to synchronization and control functionalities to ensure reliable decoding.

The LTC signal is modulated using Biphasic Mark Code (BMC) [20]. BMC is a self-clocking line-coding scheme that ensures regular signal transitions for reliable clock recovery. A binary zero is represented by a single transition at the beginning of the bit period. A binary one is represented by two transitions, one at the beginning and one at the midpoint of the bit interval. Because LTC is transmitted continuously, the resulting bit rate directly depends on the selected video frame rate. For example, at 30 fps, an 80-bit LTC frame results in a bit rate of 2400 bit/s. This corresponds to a signal frequency of 2400 Hz for binary zeros and 4800 Hz for binary ones.

A fundamental limitation of LTC is its limited temporal alignment accuracy relative to the actual camera frame capture time. This limitation arises because the TCG and the camera operate independently, without direct communication or hardware synchronization. The TCG outputs the LTC signal continuously, independent of the camera’s internal frame capture cycle. During post-processing, decoding software typically assigns the nearest available time code to each video frame. Consequently, the assigned timestamp may differ by up to half a frame period and still be considered synchronized [13].

III. TIMECODE GENERATOR

The TCG presented in this article comprises a custom hardware platform and dedicated firmware that implement GNSS-based time synchronization and LTC signal generation via deterministic General-Purpose Input/Output (GPIO) toggling.

A. Hardware

The Timecode Generator is designed for outdoor field operation. It is powered by replaceable batteries to avoid long charging times during deployment. The device has a total mass of 53.9 g, including batteries, and dimensions of $28 \times 66 \times 24$ mm. This compact form-factor allows integration with standard camera recording equipment. Fig. 2 shows the

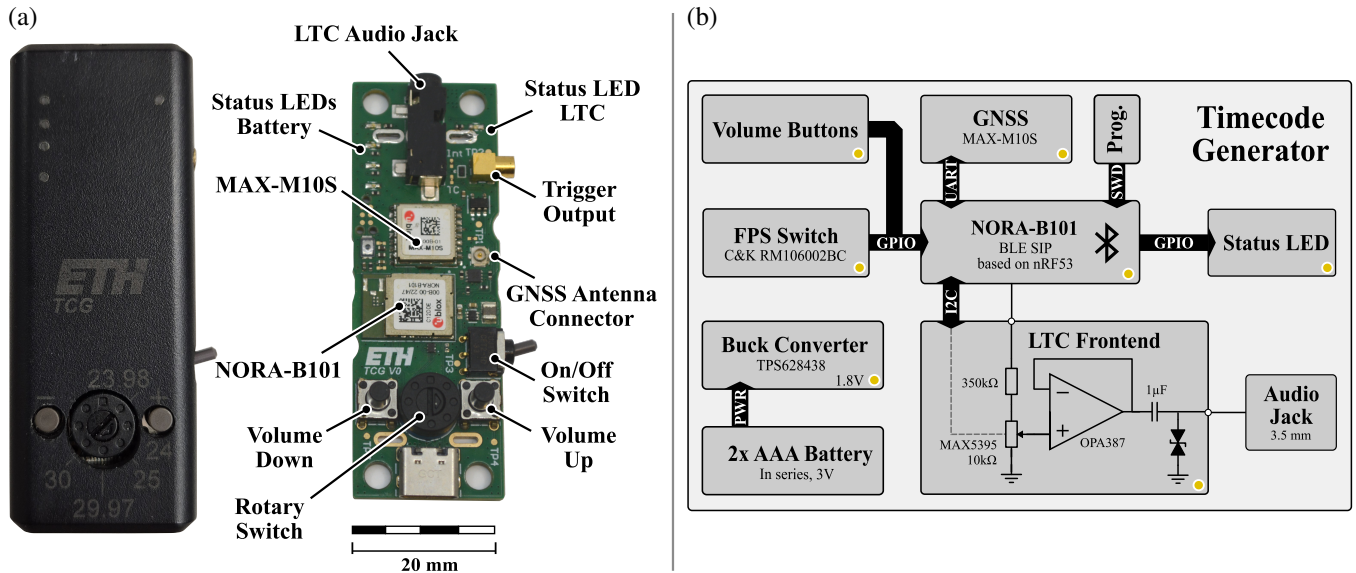


Fig. 2. System overview: (a) Top-view of enclosure and PCB of the implemented timecode generator, (b) High-level block diagram including the detailed LTC frontend sub-circuit.

hardware realization and the corresponding high-level block diagram.

1) *Processing and GNSS Timing Core*: The system is based on a *Nordic Semiconductor nRF5340* system-on-chip (SoC) featuring two ARM Cortex-M33 cores and BLE capability. The Microcontroller Unit (MCU) is integrated into a *u-blox NORA-B101* module and is responsible for creating the LTC signal. Absolute time in Coordinated Universal Time (UTC) is received via Universal Asynchronous Receiver/Transmitter (UART) from a *u-blox MAX-M10S* GNSS module. In addition, the GNSS module provides a dedicated time-pulse output that enables precise alignment to within several nanoseconds of the start of each second [21]. A *MOLEX 206560* flexible GNSS antenna is used for signal reception.

2) *LTC Output Stage*: The Society of Motion Picture and Television Engineers (SMPTE) standard for LTC signals [13] recommends LTC signal amplitudes between 1 V to 2 V and specifies an allowable range of 0.5 V to 4.5 V for professional line-level audio. However, consumer-grade microphone inputs typically operate at significantly lower signal levels, with a nominal line-level of -38 dBV [22]. Therefore, a dedicated output stage is required to attenuate the MCU-generated digital signal of 1.8 V to a range between 1 mV and 50 mV. Signal attenuation is implemented using a voltage divider consisting of a 350 k Ω resistor and an *Analog Devices MAX5395* programmable digital potentiometer with an end-to-end resistance of 10 k Ω , controlled via Inter-Integrated Circuit (I2C). The scaled signal is taken from the potentiometer's wiper terminal and buffered by a *Texas Instruments OPA387* Operational Amplifier (Op-Amp) configured as a voltage follower. The signal is then AC-coupled through a 1 μ F X7R/50V ceramic capacitor. Assuming a minimum camera input impedance of 1 k Ω [23], this results in a -3 dB corner frequency of 159 Hz for the high-pass filter.

The LTC signal is output through a standard 3.5 mm Tip-Ring-Sleeve (TRS) audio jack, which is commonly used

for microphone inputs. On stereo-capable devices, the signal is typically present only on the left channel. The output amplitude is adjustable via two Single-Pole Single-Throw (SPST) control buttons. A *C&K RM106002BC* six-position rotary switch allows selection of the target frame rate. An additional signal output, accessible via an Micro-Minature-Coaxial (MMCX) connector, provides a trigger signal at the start of every new second to synchronize external systems.

3) *Power Supply and Regulation*: The system is powered by two AAA alkaline batteries connected in series. The input voltage ranges from approximately 3 V when fresh to 1.9 V at the end of discharge. A *Texas Instruments TPS628438* buck converter regulates the supply to a stable 1.8 V system voltage. Five Light-Emitting Diodes (LEDs) provide operational feedback. Four LEDs indicate the battery state-of-charge, whereas the status LED blinks at 1 Hz, indicating active LTC signal generation.

4) *Mechanical Integration*: The circuit is implemented on a 4-layer PCB with a thickness of 1.6 mm using a standard layer stackup. The board outline was designed to fit the *New Age S3A-281109-K* ABS enclosure, which includes a dedicated compartment for two AAA alkaline batteries.

B. Firmware

The firmware is implemented using the Zephyr Real-Time Operating Systems (RTOS). It is designed as a fully interrupt-driven system. All time-critical operations are handled by hardware timers operating at 16 MHz and external interrupts. No continuous main processing loop is required during normal operation, ensuring deterministic timing behavior and minimal software-induced jitter.

1) *Time Synchronization and System Timing*: Time synchronization is referenced to the GNSS module via its *Timepulse* output, which marks the start of each UTC second with high temporal accuracy of 60 ns [24]. This interrupt serves as the global timing reference for the entire system. It triggers the generation of LTC frames aligned to absolute

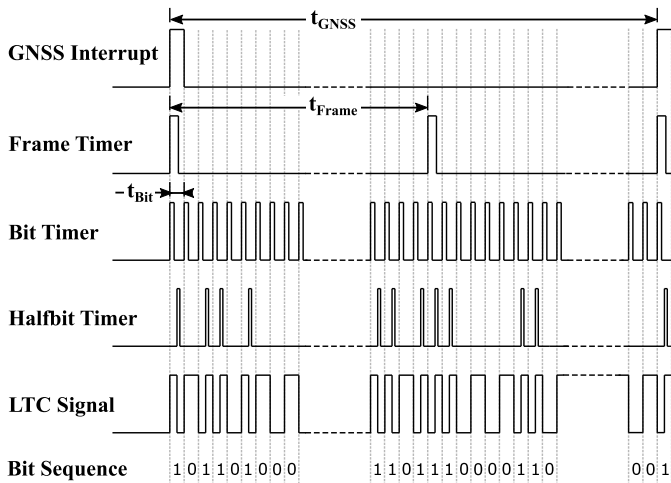


Fig. 3. Timing diagram illustrating the generation of a BMC LTC signal. An external interrupt from the GNSS module initiates the sequence generation and provides precise time synchronization. The *frame timer* defines the LTC frame duration according to the user-selected frame rate. A *bit timer* subdivides the frame into individual bit intervals, which are further subdivided by the *half-bit timer* to support bi-phase mark encoding. Based on this timing hierarchy, the LTC signal is generated by deterministic GPIO toggling. For each bit, a transition at the bit boundary is mandatory, while an additional transition at the half-bit boundary is inserted for logic ‘1’ symbols.

time and resynchronizes the internal ± 30 ppm 32 MHz crystal of the *u-blox NORA-B101* module when GNSS time synchronization is available. A hierarchical timer structure is used to generate the BMC encoded LTC signal by toggling a GPIO, as shown in Fig. 3.

2) *LTC Frame and Bit Timing Generation*: At the frame level, a dedicated *frame timer* controls the start of each LTC frame. The frame timer period is configured to match the video frame rate selected on the camera to ensure correct temporal alignment. The six-position rotary switch allows the user to select the desired frame-rate. Before signal generation begins, the complete LTC bit sequence for the upcoming frame is computed using the time information provided by the GNSS module. Each frame is subdivided by a *bit timer* that controls the timing of individual bits within the 80-bit LTC word. The bit timer toggles the LTC output GPIO pin at the beginning of each bit interval to initiate the BMC. If the transmitted bit is a logical ‘1’, the timer schedules an additional compare event at the midpoint of the bit period, referred to as *half-bit* event, which produces the second transition required by the BMC scheme. After all 80 bits of a frame have been transmitted, the bit timer is stopped and reset. It is restarted when the next frame timer event occurs.

C. System Characterization and Evaluation Procedure

This section describes the experimental procedure used to assess the temporal accuracy of the generated LTC signal. Frame rates of 24, 25, and 30 fps were analyzed to evaluate correct LTC timestamp generation. For this, a computer was synchronized to an ETH internal time Network Time Protocol (NTP) server (time.ethz.ch) and used to display UTC time at a refresh rate of 60 Hz. Measurements were conducted

TABLE I
THEORETICAL TIMING DEVIATION INTRODUCED BY THE DISCRETIZATION OF NON-INTEGER FRAME DURATIONS

FPS	1/FPS	t_{Frame}	Delay per Frame
24	41. $\bar{6}$ ms	41.666625 ms	-41.6 ns
25	40.00 ms	40.00 ms	0
30	33. $\bar{3}$ ms	33.3333125 ms	-20.8 ns

using a *Sony alpha 6400* camera with the exposure time set to 1/60 second and the TCG connected to the camera’s microphone input via a standard 3.5 mm audio cable. After the TCG achieved time synchronization and began generating LTC signals, indicated by a 1 Hz blinking of the status LED, video recording was started for one second, resulting in the same number of frames as the selected frame rate. During post-processing, timestamps were extracted from the LTC signal captured on the left audio channel and assigned to the corresponding video frames. These extracted timestamps were then compared against the UTC time displayed within each frame. Temporal alignment was quantified using the mean mismatch, which represents the systematic timing offset, and the standard deviation, which characterizes temporal variability. In addition, the mean, the Mean Absolute Error (MAE), and the Frame Shift Margin (FSM), defined as the temporal margin between the observed Maximum Absolute Error (MaxAE) and the maximum allowable time shift, were computed to characterize the deviations. Compared with the expected RMS timing uncertainty of the evaluation setup given in Eq. (1), these results can be interpreted objectively.

$$\sigma_{\text{total}} = \sqrt{\left(\frac{T_{\text{disp}}}{\sqrt{12}}\right)^2 + \left(\frac{T_{\text{exp}}}{\sqrt{12}}\right)^2} \quad (1)$$

For the equations above, it is assumed that the individual error contributions follow a uniform distribution. T_{disp} denotes the display refresh period and T_{exp} the camera exposure time.

D. Timing Analysis

To achieve the required temporal precision at bit level, the hardware timer is operated at its maximum frequency of 16 MHz, corresponding to a timing resolution of 62.5 ns per timer tick. Depending on the selected video frame rate, this finite resolution introduces a deterministic timing deviation due to the discretization of non-integer frame durations. The resulting per-frame deviations are summarized in Table I. In addition to discretization effects, timing accuracy is influenced by the frequency stability of the 32 MHz crystal oscillator integrated in the *u-blox NORA-B101* module. The crystal has a specified relative frequency accuracy of ± 30 ppm. Furthermore, a fixed computational latency is introduced by the generation of the LTC bit sequence for each frame. The maximum duration for which the system can remain synchronized without active GNSS time updates is defined as the point at which the accumulated timing error reaches half of a video frame period. This limit corresponds to the accepted temporal alignment

TABLE II
MISMATCH, MEAN ABSOLUTE ERROR (MAE), AND FRAME SHIFT MARGIN (FSM) FOR DIFFERENT FRAME RATES OVER N FRAMES

FPS	$t_{\max \text{ shift}}$	N	Mean	MAE	FSM
24	28.8 $\bar{3}$ ms	24	-1.88 ms	4.88 ms	19.83 ms
25	20.00 ms	25	-5.92 ms	7.2 ms	1.24 ms
30	16. $\bar{6}$ ms	30	6.43 ms	7.03 ms	1.18 ms

bound of LTC. Considering all relevant timing contributions, the upper bound on uninterrupted synchronization time is computed using Eq. (2):

$$t_{\max} = \frac{t_{\text{half}} - t_{\text{calc}}}{\epsilon_{\text{frame}} \cdot f_{\text{fps}} + \delta_{\text{ppm}} \cdot 10^{-6}} \quad (2)$$

Here, t_{calc} denotes the fixed computation latency, ϵ_{frame} represents the worst-case per-frame timing deviation due to timer discretization, f_{fps} is the video frame rate, and δ_{ppm} denotes the relative frequency error of the crystal oscillator in parts per million.

E. Power Analysis

Power measurements were conducted using the *Nordic Semiconductor nRF Power Profiler Kit II*. To assess total system power consumption, the profiler operated in source-meter mode. For more granular analysis, the current of the active components has been measured using the profiler’s ampere meter mode. All measurements were performed at a constant voltage of 1.8 V.

IV. RESULTS

The resulting metrics for all evaluated frame-rates over N frames are summarized in Table II. A representative section of the continuous LTC signal generated by the timecode generator is shown in Fig. 4.

The comparison between LTC signal and the UTC time reference exhibits a maximum mean offset of up to 6.43 ms with a standard deviation of 7.03 ms at 30 fps. Relating the results in Table II to the expected RMS timing uncertainty of 6.8 ms derived in Eq. (1) shows that the observed results lie within the expected uncertainty of the evaluation setup. Across all evaluated frame rates, the FSM remains greater than 1.18 ms, indicating sufficient margin to avoid frame-index ambiguity. As specified in the SMPTE standard [13], LTC encodes time on a per-frame basis and cannot guarantee temporal alignment below half the duration of one frame, as no direct synchronization exists between the camera and the TCG. In such cases, the decoding software assigns the nearest LTC timestamp to each frame, which induces bounded timing deviations. Overall, all tested frame rates satisfy the temporal accuracy requirements typically expected in professional video applications [13]. The results indicate consistent and stable synchronization of the generated LTC signal to the UTC timebase under the evaluated conditions.

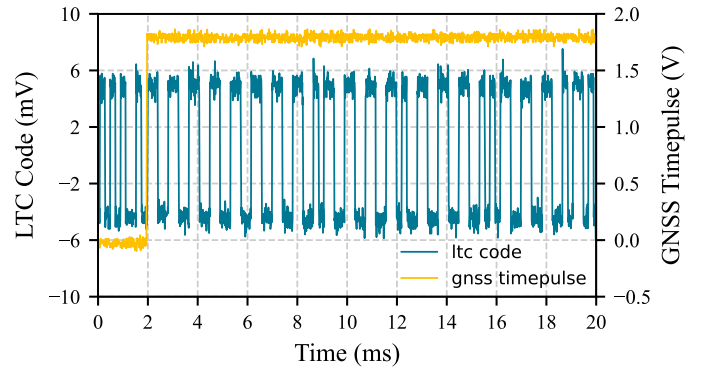


Fig. 4. Sequence of the generated LTC signal at 30 fps. The rising edge of each GNSS timepulse triggers a temporal realignment of the LTC code,

A. Timing Stability

Applying the timing model described in Section III-E, the achievable synchronization duration without active GNSS correction was evaluated for common video frame rates. For a frame rate of 24 fps, the system remains time-aligned for up to 682 s. At 25 fps, the corresponding upper bound is 654 s. The shortest synchronization interval occurs at 30 fps, where time alignment is maintained for up to 543 s, equivalent to approximately 9 min, before a potential frame-level timestamp shift may occur. These limits are dominated by the relative frequency error of the internal crystal oscillator rather than by timer discretization effects or computation latency. The deterministic timing deviation introduced by frame discretization remains negligible in comparison. The achievable synchronization duration can be substantially extended by replacing the internal crystal oscillator with a temperature-compensated crystal oscillator. This improvement would come at the cost of increased power consumption and system complexity.

B. Power Consumption

The power analysis presented in Section III-E yields the current consumption values summarized in Table III.

TABLE III
POWER CONSUMPTION OF ACTIVE COMPONENTS AT 1.8 V

Component	Part Name	Power Consumption
GNSS Module	MAX-M10S	30.92 mW
Microcontroller	NORA-B101	3.74 mW
Output Buffer	OPA387	730.8 μ W
Digital Potentiometer	MAX5395	26.52 μ W
Full system		35.37 mW

The total system power consumption at 1.8 V amounts to 35.37 mW. A current draw of 12.88 mA at 3 V corresponds to an average buck-converter efficiency of 91.5%, which is consistent with the datasheet specifications. Assuming a nominal capacity of 1000 mAh for standard AAA alkaline batteries [25], the system achieves an operating time of up to 75 h.

V. CONCLUSION

This work presents a compact and lightweight Timecode Generator that generates LTC signals for video timestamping directly from GNSS-derived time. In combination with GNSS-enabled body-attached sensor nodes, this approach enables precise temporal alignment of video recordings and sensor data without requiring direct coordination between devices. Cameras and sensor nodes operate independently and align their data streams using a common, satellite-provided time reference. Therefore, the camera and sensor nodes can be powered on immediately before the activity of interest and synchronized directly to the GNSS time base. This reduces active time and overall power consumption across all system components, enabling smaller batteries and lighter hardware while improving usability in field deployments. A detailed timing analysis quantified the individual contributions of timer discretization, computation latency, and oscillator frequency drift. The results indicate that discretization-induced deviations on the TCG side are negligible compared to the crystal oscillator's inherent frequency error. Furthermore, with a worst-case frame shift margin of 1.18 ms at 30 fps, the system is well within the permissible half-frame tolerance defined by the LTC specification.

When losing GNSS synchronization the TCG relies on the internal clock for LTC timecode generation. In this case, temporal alignment is maintained for a minimum of 543 s (9 min) at 30 fps. After this period, a frame-level timestamp shift may occur, introducing a one-frame temporal offset between the sensor data and the video stream. With an average power consumption of 35.37 mW, the system achieves a runtime of up to 75 h when powered from two standard AAA alkaline batteries.

Future work will integrate the TCG into a sports data collection scenario to evaluate its performance and usability as a visual reference for data analysis. Additionally, a more precise reference clock will be explored to extend offline synchronization time.

ACKNOWLEDGMENT

This work was supported in part by the CHIST-ERA project "SNOW" (Grant 209675) and the Ambizione Grant 233457.

REFERENCES

- [1] J. Li *et al.*, "Real-time hand gesture tracking for human-computer interface based on multi-sensor data fusion," *IEEE Sensors Journal*, vol. 21, no. 23, pp. 26 642–26 654, 2021, doi: 10.1109/JSEN.2021.3122236.
- [2] Y. Gu *et al.*, "A flexible sensor and mimu-based multisensor wearable system for human motion analysis," *IEEE Sensors Journal*, vol. 23, no. 4, pp. 4107–4117, 2023, doi: 10.1109/JSEN.2022.3233653.
- [3] M. Zaltieri *et al.*, "Assessment of a multi-sensor fbg-based wearable system in sitting postures recognition and respiratory rate evaluation of office workers," *IEEE Transactions on Biomedical Engineering*, vol. 70, no. 5, pp. 1673–1682, 2023, doi: 10.1109/TBME.2022.3225065.
- [4] T. A. Swain *et al.*, "The role of multi-sensor measurement in the assessment of movement quality: A systematic review," *Sports Medicine*, vol. 53, no. 12, pp. 2477–2504, 2023, doi: 10.1007/s40279-023-01905-1.
- [5] F. Salis *et al.*, "A multi-sensor wearable system for the assessment of diseased gait in real-world conditions," *Frontiers in Bioengineering and Biotechnology*, vol. 11, p. 1143248, 2023, doi: 10.3389/fbioe.2023.1143248.
- [6] Y. Lu *et al.*, "Effective recognition of human lower limb jump locomotion phases based on multi-sensor information fusion and machine learning," *Medical & Biological Engineering & Computing*, vol. 59, pp. 883–899, 2021, doi: 10.1007/s11517-021-02335-9.
- [7] C. Y. Kim *et al.*, "Wireless technologies for wearable electronics: a review," *Advanced Electronic Materials*, p. 2400884, 2025.
- [8] R. Ohara *et al.*, "Microsync: Sub-micro second accuracy wireless time synchronization service," *IEEE Access*, vol. 12, pp. 124 478–124 494, 2024, doi: 10.1109/ACCESS.2024.3446668.
- [9] T. Polonelli *et al.*, "A self-sustainable and micro-second time synchronized multi-node wireless system for aerodynamic monitoring on wind turbines," *IEEE Access*, vol. 11, pp. 119 506–119 522, 2023, doi: 10.1109/ACCESS.2023.3327422.
- [10] N. Krull *et al.*, "Wireless low-latency synchronization for body-worn multi-node systems in sports," in *2025 IEEE 21st International Conference on Body Sensor Networks (BSN)*, 2025, pp. 1–4, doi: 10.1109/BSN66969.2025.11337444.
- [11] T. Kulvicius *et al.*, "Deep learning empowered sensor fusion boosts infant movement classification," *Communications Medicine*, vol. 5, p. 16, 2025, doi: 10.1038/s43856-024-00701-w.
- [12] J. F. Hafer *et al.*, "Challenges and advances in the use of wearable sensors for lower extremity biomechanics," *Journal of Biomechanics*, vol. 157, p. 111714, 2023, doi: 10.1016/j.jbiomech.2023.111714.
- [13] S. of Motion Picture and T. Engineers, "Smpte st 12-1:2014 - time and control code," 2014, accessed: 2025-17-12. [Online]. Available: <https://pub.smpte.org/doc/st12-1/20140220-pub/>.
- [14] Tentacle Sync, "Tentacle sync e timecode generator," <https://tentaclesync.com/products/sync-e>, Tentacle Sync, 2025, accessed: 2025-12-18.
- [15] Atomos, "Atomos ultrasync blue wireless timecode sync," <https://www.atomos.com/product/ultrasync-blue/>, Atomos, 2025, accessed: 2025-12-18.
- [16] Deity Microphones, "Deity tc-1 timecode box," <https://deitymic.com/products/tc-1-timecode-box/>, Deity Microphones, 2025, accessed: 2025-12-18.
- [17] L. Schulthess *et al.*, "Skilog: A smart sensor system for performance analysis and biofeedback in ski jumping," in *2023 IEEE Biomedical Circuits and Systems Conference (BioCAS)*, 2023, pp. 1–5, doi: 10.1109/BioCAS58349.2023.10389124.
- [18] M. Salimnejad, N. Pappas, and M. Kountouris, "So timely, yet so stale: The impact of clock drift in real-time systems," *IEEE Communications Letters*, vol. 29, no. 10, pp. 2228–2232, 2025, doi: 10.1109/LCOMM.2025.3590865.
- [19] R. Gareus and contributors, "libltc: Linear/longitudinal timecode library," <https://github.com/x42/libltc>, 2022, version 1.3.2, LGPL-3.0 License. [Online]. Available: <https://github.com/x42/libltc>.
- [20] K. S. Mohamed, "Wireless communication systems: Line coding, modulation, multiple access, and duplexing," in *Synthesis Lectures on Engineering, Science, and Technology*. Springer, 2022, pp. 101–132.
- [21] u-blox AG, *GPS-based Timing: Considerations with u-blox 6 GPS receivers*, Application Note, u-blox AG, Zürcherstrasse 68, 8800 Thalwil, Switzerland, 2011, application Note, Document No. GPS.G6-X-11007, Preliminary. [Online]. Available: https://content.u-blox.com/sites/default/files/products/documents/Timing_AppNote_%28GPS.G6-X-11007%29.pdf.
- [22] S. Adorno, F. Cerini, and F. Vercesi, "Microphones," in *Silicon Sensors and Actuators*, B. Vigna *et al.*, Eds. Springer, 2022, [Online]. Available: https://doi.org/10.1007/978-3-030-80135-9_15.
- [23] *Sound system equipment – Part 4: Microphones*, International Electrotechnical Commission Std. IEC 60 268-4, 2018, specifies measurement methods for electrical impedance, sensitivity, and other characteristics of sound system microphones. [Online]. Available: <https://webstore.iec.ch/publication/32039>.
- [24] u-blox AG, *MAX-M10S Data Sheet: Standard precision GNSS module*, Product Data Sheet, u-blox AG, Zürcherstrasse 68, 8800 Thalwil, Switzerland, 2025, data Sheet, Document No. UBX-20035208, Revision R07 (29 Oct 2025). [Online]. Available: https://content.u-blox.com/sites/default/files/MAX-M10S_DataSheet_UBX-20035208.pdf.
- [25] K. Mikhaylov and J. Tervonen, "Experimental evaluation of alkaline batteries's capacity for low power consuming applications," in *2012 IEEE 26th International Conference on Advanced Information Networking and Applications*, 2012, pp. 331–337, doi: 10.1109/AINA.2012.99.